Supporting Information

Tailoring Surface of Natural Graphite with Functional Metal Oxides via a Facile Crystallization for Lithium-ion Batteries

Jun Won Lee[‡], So Yeun Kim[‡], Dong Young Rhee, Sungmin Park, Jae Yup Jung, Min-Sik Park*

Department of Advanced Materials Engineering for Information and Electronics, Integrated Education Institute for Frontier Science & Technology (BK21 Four), Kyung Hee University, 1732 Deogyeong–daero, Giheung–gu, Yongin 17104, Republic of Korea

‡These authors contributed equally.

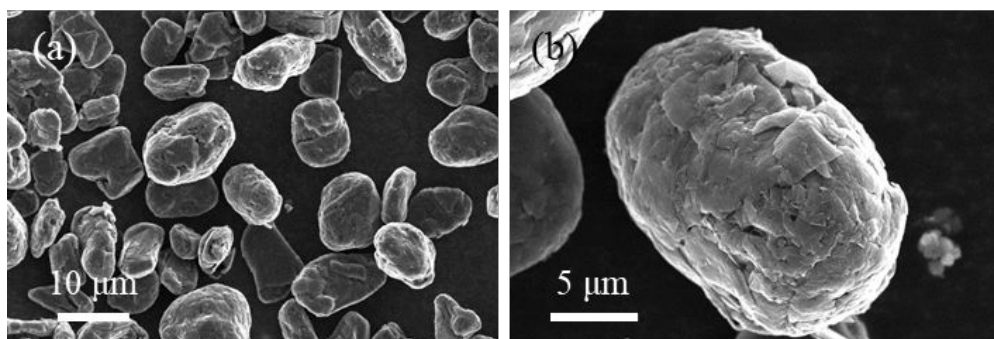*Corresponding author : mspark@khu.ac.kr (M-S. Park)

Figure S1. (a) Low-magnification and (b) high-magnification FESEM images of pristine NG.
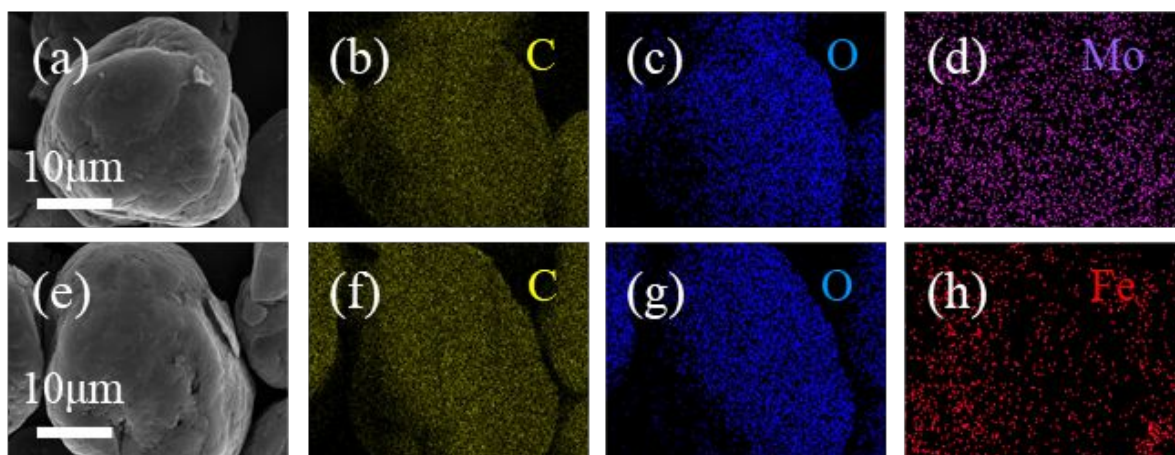
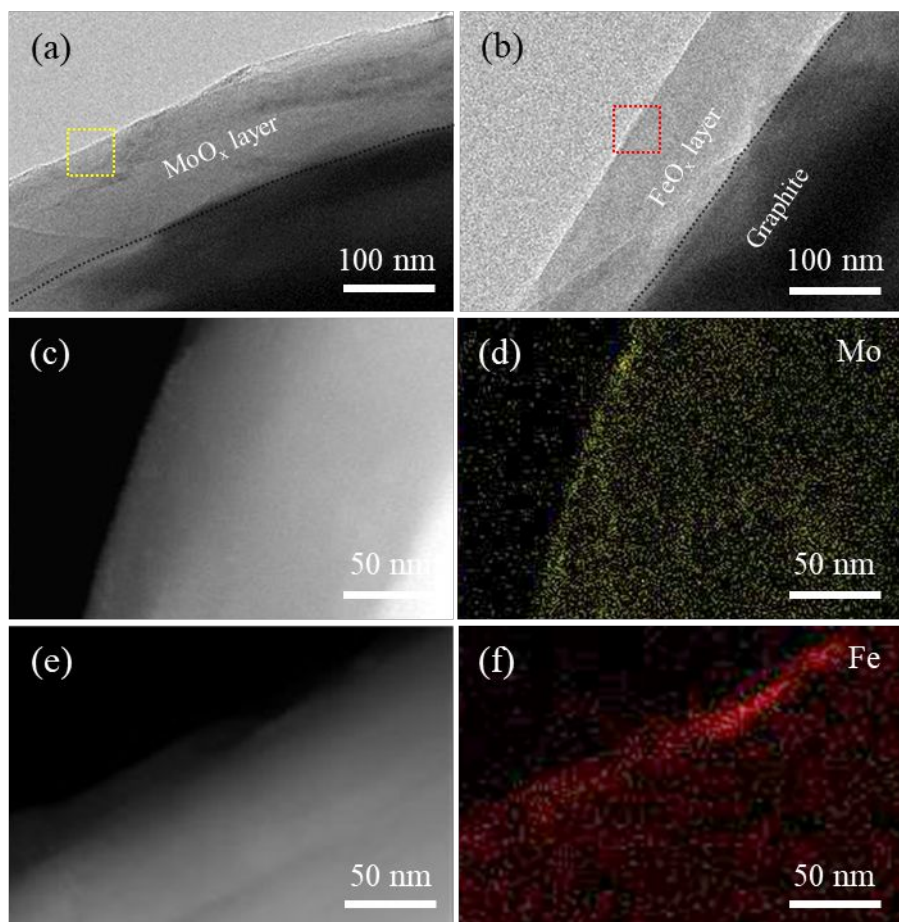Figure S2. Corresponding EDS elemental mapping results of (a-d) a-MoO$_x$-NG and (e-h) a-FeO$_x$-NG particles.

Figure S3. TEM images of (a) a-MoO$_x$–NG and (b) a-FeO$_x$–NG. Dark-field TEM images and corresponding elemental mapping of (c, d) a-MoO$_x$–NG and (e, f) a-FeO$_x$–NG; molybdenum (Mo, yellow) and iron (Fe, red)
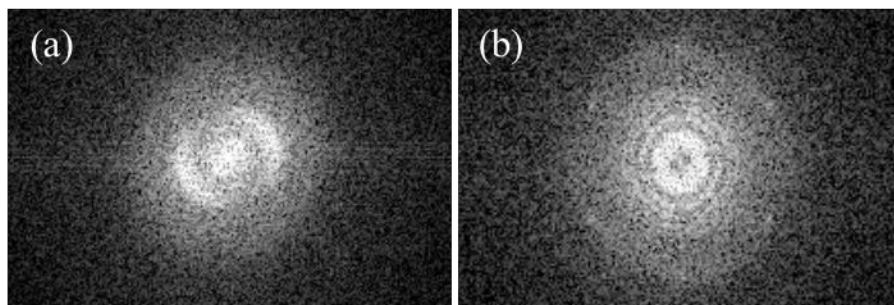
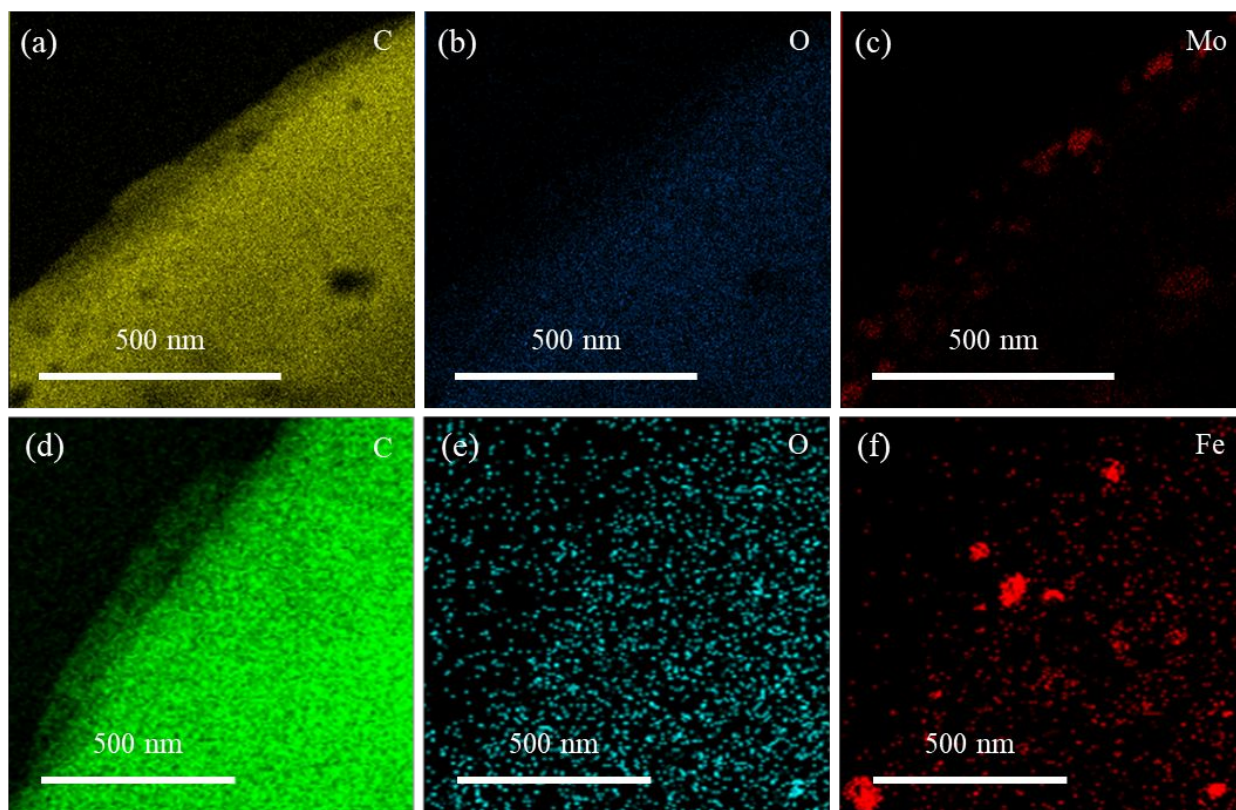Figure S4. FFT patterns taken from the amorphous regions of (a) c-MoO$_2$-NG and (b) c-Fe$_3$O$_4$-NG.

Figure S5. Corresponding EDS elemental mapping results of (a-c) c-MoO$_2$-NG and (d-f) c-Fe$_3$O$_4$-NG prepared by a facile-crystallization process.
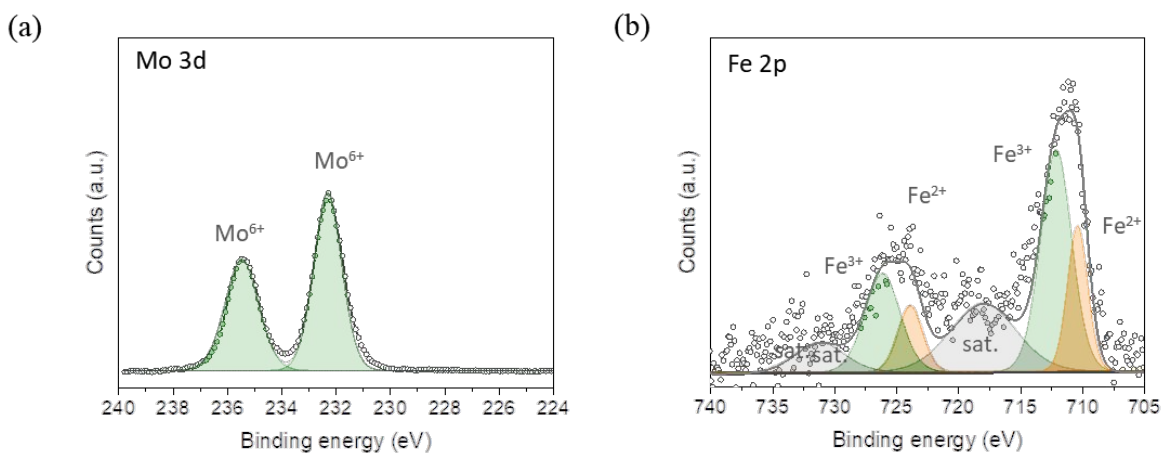
Figure S6. Deconvoluted XPS (a) Mo 3d spectra of a-MoO$_x$-NG and (b) Fe 2p spectra of a-FeO$_x$-NG composites.

Table S1. The contents of $Mo^{4+}/Mo^{5+}/Mo^{6+}$ from XPS spectrum of $a\text{-}MoO_x\text{-}NG$ and $c\text{-}MoO_2\text{-}NG$.

	a-MoO$_x$-NG			c-MoO$_2$-NG		
	$3d_{3/2}$	$3d_{5/2}$	total	$3d_{3/2}$	$3d_{5/2}$	total
Mo^{6+}	39.74	60.26	100	7.2	15.8	23.0
Mo^{5+}	-	-	-	5.1	15.6	20.7
Mo^{4+}	-	-	-	22.9	33.4	56.3

Table S2. The contents of Fe^{3+}/Fe^{2+} from XPS spectrum of a-FeO$_x$-NG and c-Fe$_3$O$_4$-NG.

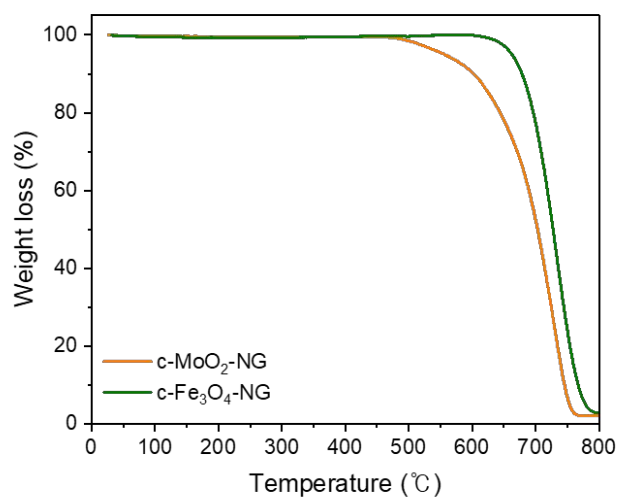|	a-FeO$_x$-NG			c-Fe$_3$O$_4$-NG		
	$2P_{1/2}$	$2P_{3/2}$	total	$2P_{1/2}$	$2P_{3/2}$	total
Fe^{3+}	30.6	42.9	73.5	23.4	45.8	69.2
Fe^{2+}	10.3	16.2	26.5	11.2	19.6	30.8

Figure S7. Thermogravimetric analysis curve of c-Fe$_3$O$_4$-NG and c-MoO$_2$-NG composite.
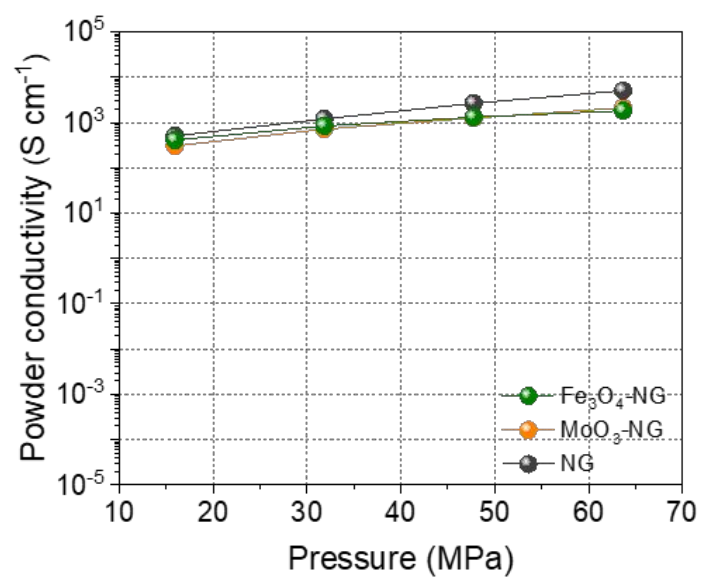
Figure S8. Powder conductivities of pristine NG, c-MoO$_2$-NG and c-Fe$_3$O$_4$-NG.

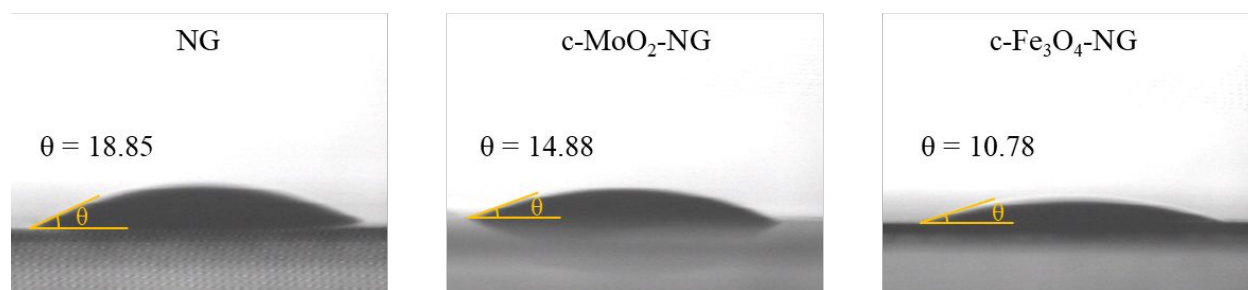| NG	c-MoO$_2$-NG	c-Fe$_3$O$_4$-NG
θ = 18.85	θ = 14.88	θ = 10.78

Figure S9. Static contact angles of pristine NG, c-MoO$_2$-NG and c-Fe$_3$O$_4$-NG anodes.
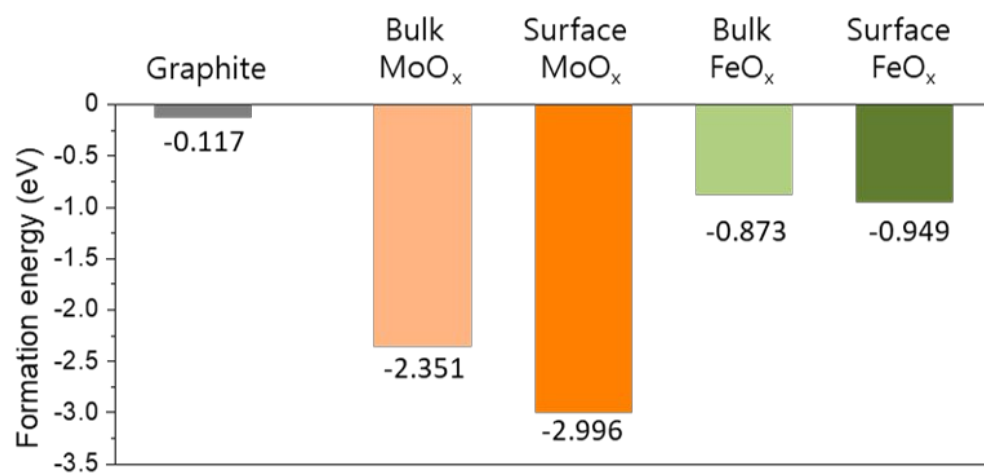
Figure S10. Comparison of calculated formation energies for Li$^+$ adsorption of MoO$_x$ and FeO$_x$.
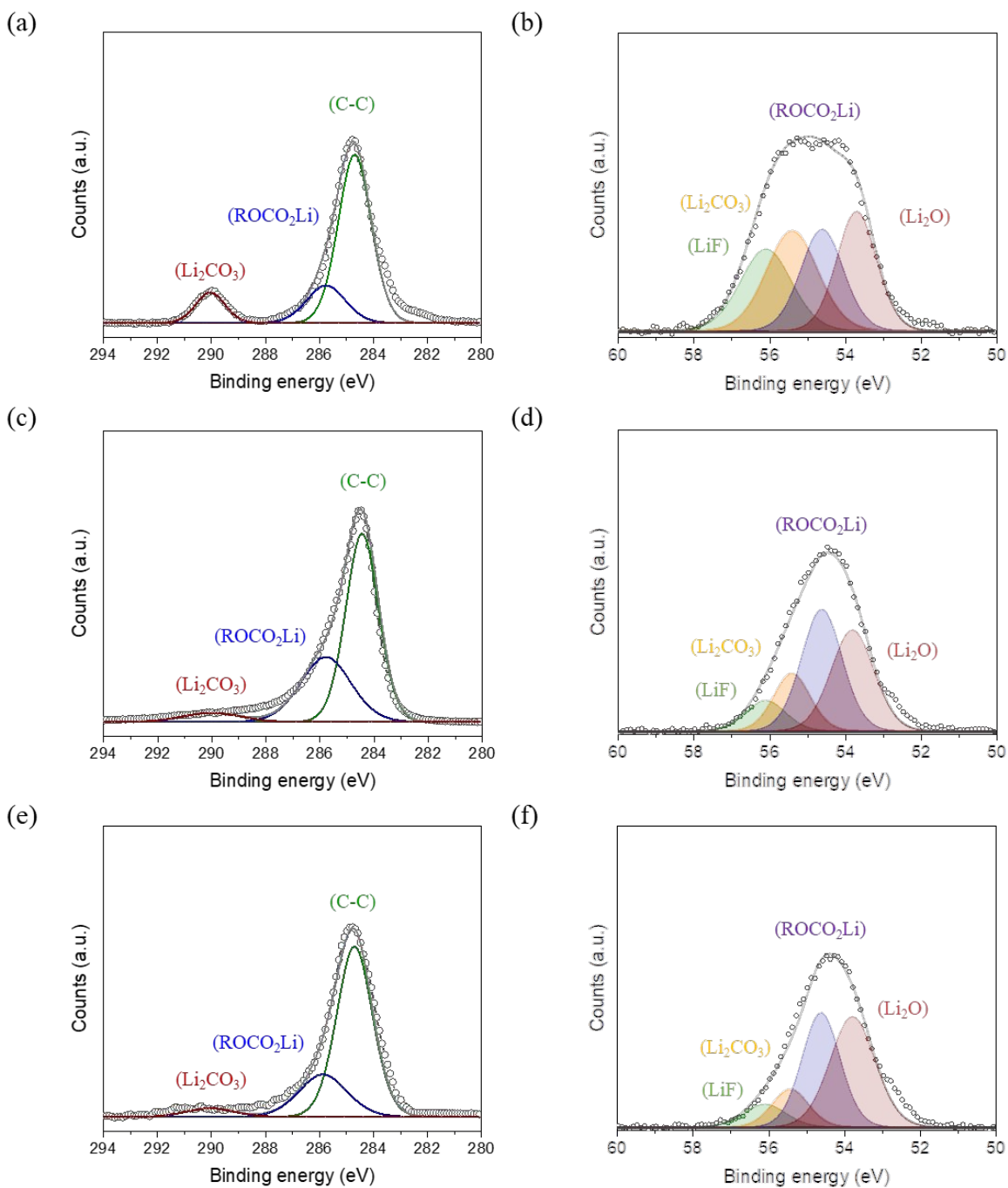
Figure S11. XPS C 1s and Li 1s spectra of (a, b) NG, (c, d) c-MoO$_2$-NG and (e, f) c-Fe$_3$O$_4$-NG anodes after cycling.

Table S3. Fitting results of the Nyquist plots using the equivalent circuit.

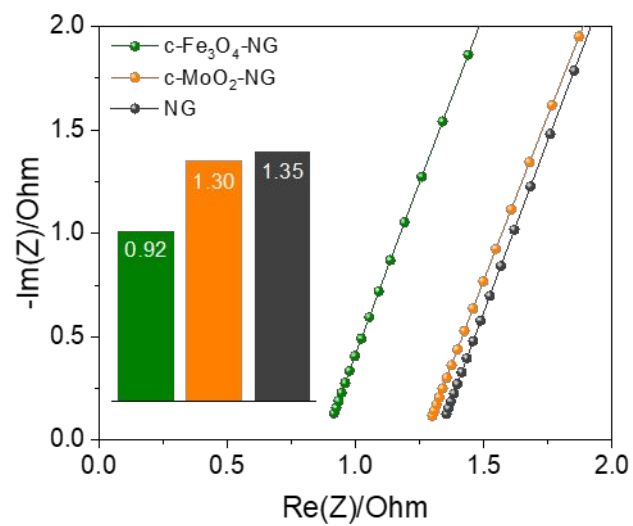|	OCV		After 1st charge		
	R_b	R_{ct}	R_b	R_{SEI}	R_{ct}
c-Fe$_3$O$_4$-NG	0.9	203.4	1.5	94.7	35.0
c-MoO$_2$-NG	1.3	217.5	2.0	75.9	29.7
Pristine NG	1.4	313.4	5.3	211.1	38.9

Figure S12. Nyquist plots for magnified high-frequency region of pristine NG, c-MoO$_2$-NG and
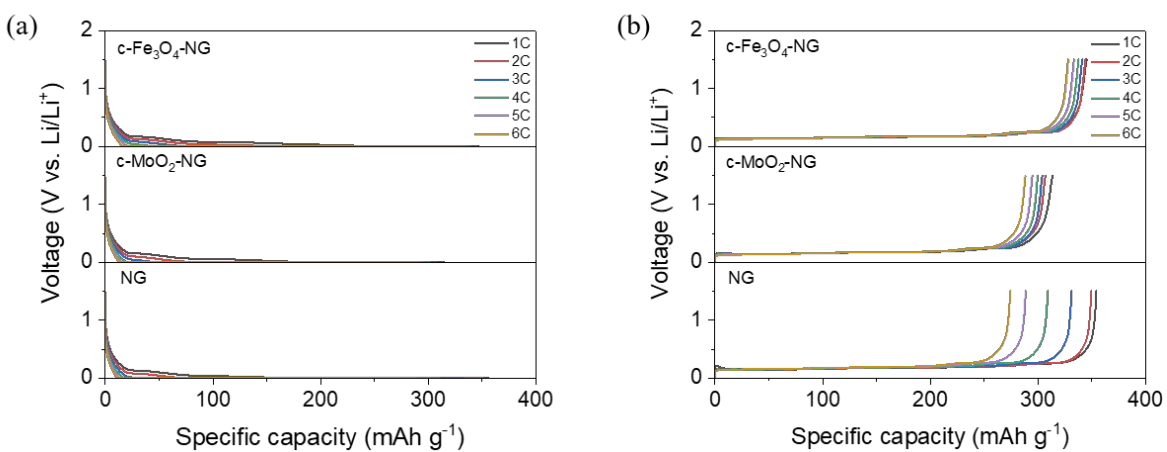
c-Fe$_3$O$_4$-NG anodes.

Figure S13. Voltage profiles during (a) charging and (b) discharging process of pristine NG, c-MoO$_2$-NG and c-Fe$_3$O$_4$-NG andodes recorded at various current densities from 1 C to 6 C.
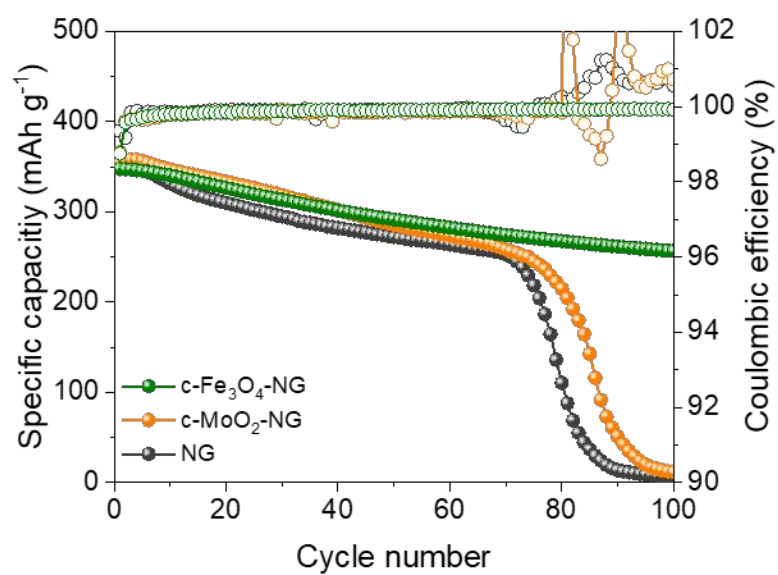
Figure S14. Cycle performance of pristine NG, c-MoO$_2$-NG and c-Fe$_3$O$_4$-NG andodes at a constant current density of 1 C for 100 cycles.
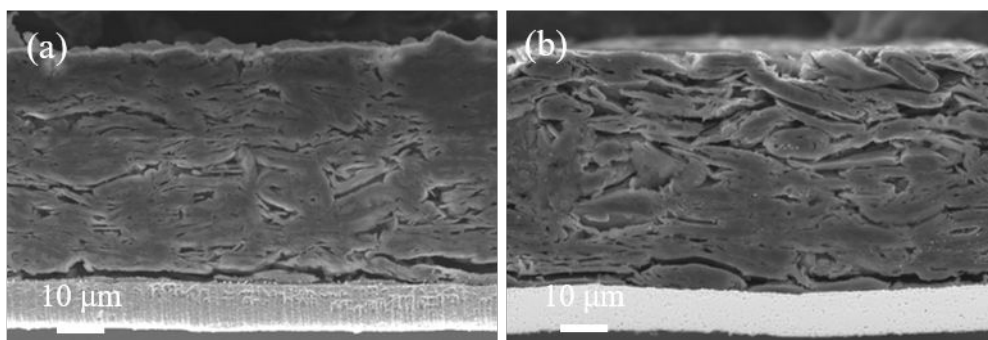
Figure S15. Cross-sectional SEM images of (a) pristine NG and (b) c-Fe$_3$O$_4$-NG anodes after the

300 cycles.